

Magnon spectrum in the domain ferromagnetic state of antisite-disordered double perovskitesSubrat Kumar Das,^{*} Viveka Nand Singh, and Pinaki Majumdar*Harish-Chandra Research Institute, Chhatnag Road, Jhusi, Allahabad 211 019, India*

(Received 19 October 2012; revised manuscript received 17 October 2013; published 26 December 2013)

In their ideal structure, double perovskites such as $\text{Sr}_2\text{FeMoO}_6$ have alternating Fe and Mo along each cubic axis, and a homogeneous ferromagnetic metallic ground state. Imperfect annealing leads to the formation of structural domains. The moments on mislocated Fe atoms that adjoin each other across the domain boundary have an antiferromagnetic coupling between them. This leads to a peculiar magnetic state, with ferromagnetic domains coupled antiferromagnetically. At a short distance the system exhibits ferromagnetic correlation while at large length scales the net moment is strongly suppressed due to interdomain cancellation. We provide a detailed description of the spin-wave excitations of this complex magnetic state, obtained within a $1/S$ expansion, for a progressively higher degree of mislocation, i.e., antisite disorder. At a given wave vector the magnons propagate at multiple energies, related, crudely, to “domain confined” modes with which they have a large overlap. We provide a qualitative understanding of the trend observed with growing antisite disorder, and contrast these results to the much broader spectrum that one obtains for uncorrelated antisites.

DOI: [10.1103/PhysRevB.88.214428](https://doi.org/10.1103/PhysRevB.88.214428)

PACS number(s): 75.30.Ds, 75.60.Ch, 75.47.Lx, 75.40.Gb

I. INTRODUCTION

Double perovskite (DP) materials with the general formula $A_2BB'O_6$ have generated a great deal of interest¹ both in terms of their basic physics as well as the possibility of technological applications. Here, B and B' are the electronically active ions, typically $3d$, $4d$, or $5d$ elements, while A is either a rare earth or an alkaline earth. The B ions are usually magnetic, e.g., Fe, Co, Ni, Cr, or Mn, while B' is typically nonmagnetic, e.g., Mo or W. In particular, $\text{Sr}_2\text{FeMoO}_6$ (SFMO) shows high ferromagnetic $T_c \sim 420$ K, large electron spin polarization (half metallicity), and significant low-field magnetoresistance.^{2,3}

In the structurally ordered materials the magnetic ordering arises from a combination of strong coupling on the B site between the large S core spin and the valence electron (preferring one electron spin polarization on site) and delocalization of the electrons on the B -O- B' network. This effective “double exchange” mechanism operates in SFMO, where the ferromagnetic (FM) coupling between the $S = 5/2$ localized magnetic moments (Fe³⁺ ion, $3d^5$ state) arises from the delocalization of electrons over the Mo-O-Fe network. The B (Fe) ions order ferromagnetically while the conduction electrons that mediate the exchange are aligned opposite to the Fe moments, leading to a saturation magnetization of $4\mu_B$ per formula unit in ordered SFMO. The physics in real materials, however, is complicated by the presence of *antisite disorder* (ASD) whereby some B ions occupy the positions of B' ions and vice versa.

There is clear evidence now that B - B' mislocations are not random but spatially correlated.^{4,5} While ASD suppresses long-range structural order, electron microscopy⁴ and x-ray absorption fine structure (XAFS)⁵ reveal that a high degree of short-range order survives. In fact, the system breaks up into locally ordered regions, phase slipped with respect to one another. The antiphase boundary consists of two similar atoms (B - B or B' - B') sitting next to each other, while within a domain the B and B' alternate in all directions. The structural disorder has a direct magnetic impact. If two Fe ions adjoin

each other, the filled shell d^5 configuration leads to a large antiferromagnetic (AFM) superexchange coupling between them, which makes two neighboring FM domains antiparallel. The result is a pattern of structural domains, with each domain internally ferromagnetic while adjoining domains are AFM with respect to each other. This naturally leads to a suppression of the bulk magnetization with growing ASD.

Domain structure has been inferred in the low doping manganites as well, due to competing FM and AFM interactions. Inelastic neutron scattering in those materials suggests the presence of FM domains in a predominantly AFM matrix, and allows a rough estimate of the domain size.^{6,7} We aim to provide a similar framework for interpreting the magnetic state and domain structure in the DP from spin-wave (SW) data.

Our main results are the following: (i) We compute the dynamical magnetic structure factor within a $1/S$ expansion of an effective Heisenberg model chosen to fit the electronic model results. (ii) The magnon data is reminiscent of the *clean limit* even at maximum ASD (50%), where the bulk magnetization vanishes due to interdomain cancellation. (iii) We suggest a rough method for inferring the domain size from the magnon data and check its consistency with the ASD configurations used. (iv) We demonstrate that *uncorrelated* ASD leads to a much greater scattering of magnons and a much broader lineshape. This suggests that, in addition to XAFS and microscopy, neutron scattering would be a sensitive probe of the nature of disorder in these materials.

The paper is organized as follows: In Sec. II we discuss the generation of the structural motif, the solution of the electronic problem, and the estimation of exchanges for an effective Heisenberg model. In Sec. III we recapitulate the spin-wave formulation for noncollinear phases and present the magnon spectrum obtained for the different disordered configurations. In Sec. IV we discuss the results, attempting to analyze the magnon spectrum for correlated antisites in terms of confined spin-wave modes, and contrasting the result to magnons in an “uncorrelated” antisite background. Section V contains our concluding remarks.

II. EFFECTIVE MAGNETIC MODEL

A. Structural motif

Given the similar location of the B and B' ions (at the center of the octahedra) the tendency towards defect formation is more pronounced in the double perovskites. This tendency of mislocation interplays with the inherent B - B' ordering tendency and creates a spatially correlated pattern of antisites^{4,5} rather than random mislocation. To model this situation we have used a simple *lattice-gas* model.⁸ On proper annealing it will go to a long-range ordered $B, B', B, B' \dots$ pattern. We frustrate this by using a short annealing time to mimic the situation in the real materials. We encode the atomic positions by defining a binary variable η_i , such that $\eta_i = 1$ when a site has a B ion, and 0 when it has a B' ion. Thus for an ordered case we will get η 's as 1,0,1,0,1,0, ... along each cubic axis. The B - B' patterns that emerge on short annealing are characterized by the structural order parameter $S = 1 - 2x$, where x is the fraction of B (or B') atoms that are on the wrong sublattice. We have chosen four disordered families with increasing disorder for our study. Each member of the disordered family is being generated at a given annealing temperature for a fixed annealing time, starting with different initial random B - B' configurations. One structural motif each for these families is shown in the first column of Fig. 1, with progressively increasing disorder (from top to bottom) on a 40×40 lattice. We plot $g(\mathbf{r}_i) = (\eta_i - \frac{1}{2})e^{i\pi(x_i+y_i)}$ as an indicator of structural order. For a perfectly ordered structure $g(\mathbf{r}_i)$ is constant. We denote these different realizations of antisite-disordered configurations as C1, C2, C3, and C4, and the corresponding structural order parameter has values $S = 0.98, 0.86, 0.59,$ and 0.17 , respectively, from top to bottom in the first column. We solve the electronic-magnetic problem on these structural motifs.

B. Electronic Hamiltonian

To study the magnetic order we use the electronic-magnetic Hamiltonian that has the usual couplings of the ordered double perovskite, and an additional AFM coupling when two magnetic B ions are nearest neighbor (NN). The Hamiltonian for the microscopic model is

$$H = H_{\text{loc}}\{\eta\} + H_{\text{kin}}\{\eta\} + H_{\text{mag}}\{\eta\}. \quad (1)$$

$H_{\text{loc}}\{\eta\} = \epsilon_B \sum_{i,\sigma} \eta_i f_{i\sigma}^\dagger f_{i\sigma} + \epsilon_{B'} \sum_{i,\sigma} (1 - \eta_i) m_{i\sigma}^\dagger m_{i\sigma}$ is the on-site term, where ϵ_B and $\epsilon_{B'}$ are level energies at the B and B' sites, respectively. Here, f is the electron operator referring to the magnetic B site and m is that of the nonmagnetic B' site.

$H_{\text{kin}}\{\eta\} = -t_1 \sum_{\langle ij \rangle, \sigma} \eta_i \eta_j f_{i\sigma}^\dagger f_{j\sigma} - t_2 \sum_{\langle ij \rangle, \sigma} (1 - \eta_i)(1 - \eta_j) m_{i\sigma}^\dagger m_{j\sigma} - t_3 \sum_{\langle ij \rangle, \sigma} (\eta_i + \eta_j - 2\eta_i \eta_j) (f_{i\sigma}^\dagger m_{j\sigma} + \text{H.c.})$ represents the NN hopping term. For simplicity we set all the NN hopping amplitudes to be the same $t_1 = t_2 = t_3 = t$. The magnetic interaction term $H_{\text{mag}}\{\eta\} = J \sum_{i,\alpha,\beta} \eta_i \mathbf{S}_i \cdot f_{i\alpha}^\dagger \vec{\sigma}_{\alpha\beta} f_{i\beta} + \tilde{J}_{\text{AF}} \sum_{\langle ij \rangle} \eta_i \eta_j \mathbf{S}_i \cdot \mathbf{S}_j$ consists of the electron-spin coupling J on B sites, and AFM superexchange coupling \tilde{J}_{AF} between two NN magnetic B sites. \mathbf{S}_i is the classical core spin on the B site at \mathbf{r}_i with $|\mathbf{S}_i| = 1$. We take $J/t \gg 1$ with $J > 0$ and $\tilde{J}_{\text{AF}}|\mathbf{S}|^2/t = 0.08$, based on the T_N scale in SrFeO_3 . We have ignored orbital degeneracy, Coulomb effects, etc.,

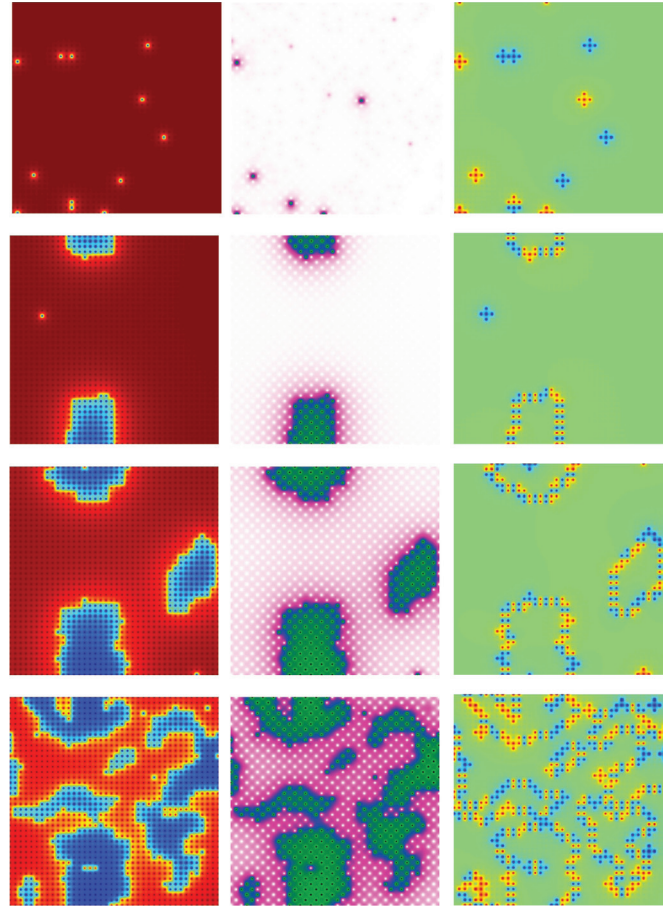


FIG. 1. (Color online) The first column contains the structural motif for four disordered families (C1–C4) with progressively increasing disorder ($S = 0.98, 0.86, 0.59,$ and 0.17) from top to bottom. We plot $g(\mathbf{r}_i) = (\eta_i - \frac{1}{2})e^{i\pi(x_i+y_i)}$. The second column shows the ground state spin overlap factor, $h_i = \mathbf{S}_0 \cdot \mathbf{S}_i$, where \mathbf{S}_0 is the lower-left-corner spin in the lattice. In the third column, we have shown the corresponding NN bond configurations. Here, red, blue, and green represent B - B , B' - B' , and B - B' bonds, respectively. The lattice size is 40×40 (Ref. 9).

to focus on the essential magnetic model on the disordered structure. We will use a two-dimensional (2D) model because it already captures the qualitative physics while allowing ease of visualization and access a large system size. The formulation readily carries over to three dimensions as well.

We have used a real space exact diagonalization based Monte Carlo method involving a traveling cluster approximation¹⁰ to anneal the spin-fermion system towards its ground state in the disordered background.⁹

Annealing the electron-spin system down to low temperature on a given structural motif leads to the magnetic ground states shown in the middle column of Fig. 1. We plot the spin overlap factor, $h_i = \mathbf{S}_0 \cdot \mathbf{S}_i$, where \mathbf{S}_0 is the lower-left-corner spin in the lattice. The comparison of the first and second columns in Fig. 1 indicates that the structural and magnetic domains coincide with each other. The third column of Fig. 1 shows the NN structural patterns. We have three possibilities, B - B , B' - B' , and B - B' , represented by the colors red, blue, and green, respectively, in the plot.

C. Effective Heisenberg Hamiltonian

Doing a SW analysis for domain ferromagnetic DP materials using the full electronic-magnetic Hamiltonian [Eq. (1)] is difficult. Further, in a clean SFMO system the SW excitations are well described by the Heisenberg model with NN and next nearest neighbor (NNN) interactions and the quantum corrections of order $1/S^2$ to the magnon spectrum are small.¹¹ So we assume that the spin dynamics can be described by an *effective* Heisenberg model

$$H_{\text{eff}} = \sum_{\langle ij \rangle} J_{ij} \mathbf{S}_i \cdot \mathbf{S}_j, \quad (2)$$

where $\{ \}$ represents the set of NN and NNN sites. J_{ij} is the effective coupling (FM/AFM) between the local moments at the \mathbf{r}_i and \mathbf{r}_j sites. In our 2D ASD configurations J_F operates between two local moments when they are at the NNN position and J_{AF} is active when the moments are at the NN position (a B - O - B arrangement). We have estimated the effective couplings J_F and J_{AF} as follows. For getting the FM coupling (J_F) we have considered the ordered double perovskite structure. We calculated the order parameter, i.e., the magnetic structure factor $D(\mathbf{k})$ at $\mathbf{k} = (0,0)$, as a function of temperature for the full electronic Hamiltonian [Eq. (1)] using Monte Carlo simulation. We then repeated the same procedure for the NNN FM Heisenberg Hamiltonian, defined on only the magnetic sites of the double perovskite. We find that for $J_F/t = -0.04$, the two results match very well.

In order to get the AFM coupling we considered the ordered perovskite where both the B and B' sites carry a magnetic moment (mimicking SrFeO_3), and computed its AFM structure factor peak $\mathbf{k} = (\pi, \pi)$. This model involves both electronic kinetic energy and Fe-Fe superexchange. We find that the result can be modeled via a Heisenberg model with $J_{AF}/t = 0.065$.

Using the couplings inferred from these limiting cases, $J_F/t = -0.04$ and $J_{AF}/t = 0.065$, we studied the bond-disordered Heisenberg model for the antisite-disordered DP magnets. We compared the FM structure factor peak $D(\mathbf{k})$ at $\mathbf{k} = (0,0)$ obtained from the disordered Heisenberg model with that from the full electronic Hamiltonian [Eq. (1)]. The Heisenberg result for the FM structure factor $D(0,0)$ as a function of temperature matches very well (Fig. 2) with the electronic Hamiltonian result for all ASD configurations. This gives us confidence in the usefulness of the Heisenberg model for spin dynamics.

III. SPIN DYNAMICS

A. Spin-wave excitations

In this section we use the spin rotation technique¹² to evaluate the SW modes and dynamical structure factor at zero temperature. The effective Heisenberg model [Eq. (2)] can be cast in a form useful for SW analysis by defining a *local frame* at each site so that the spins point along the $+z$ direction in the ground state. We can use $\tilde{\mathbf{S}}_i = U_i \mathbf{S}_i$, where $\tilde{\mathbf{S}}_i$ points along its local z axis in the classical limit. The unitary rotation matrix

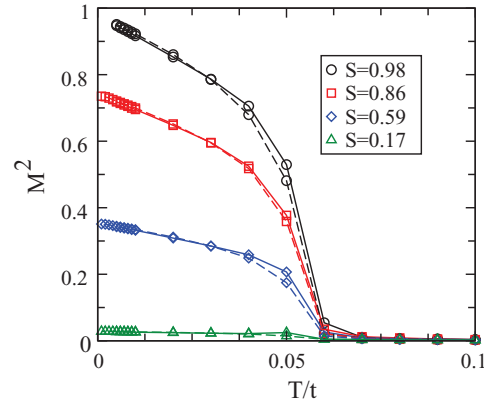


FIG. 2. (Color online) Comparison between the evolution of the spin-structure factor $D(\mathbf{k})$ at $\mathbf{k} = (0,0)$ with temperature for the spin configurations of various disordered families (from top to bottom) C1, C2, C3, and C4 obtained from the full electronic Hamiltonian with $\tilde{J}_{AF}S^2/t = 0.08$ and the effective Heisenberg model with $J_F/t = -0.04$ and $J_{AF}/t = 0.065$. The lattice size is 40×40 .

U_i for site \mathbf{r}_i is given by

$$U_i = \begin{vmatrix} \cos(\theta_i) \cos(\psi_i) & \cos(\theta_i) \sin(\psi_i) & -\sin(\theta_i) \\ -\sin(\psi_i) & \cos(\psi_i) & 0 \\ \sin(\theta_i) \cos(\psi_i) & \sin(\theta_i) \sin(\psi_i) & \cos(\theta_i) \end{vmatrix}, \quad (3)$$

where θ and ψ are the Euler rotation angles. Now one can write the generalized Hamiltonian

$$H_{\text{eff}} = \sum_{\langle ij \rangle} J_{ij} \tilde{\mathbf{S}}_i \cdot F_{ij} \tilde{\mathbf{S}}_j, \quad (4)$$

where $F_{ij} = U_i U_j^{-1}$ is the overall rotation from one reference frame to another and its elements $F_{ij}^{\alpha\beta}$ can be obtained from Eq. (3).

Applying the approximate Holstein-Primakoff (HP) transformation in the large S limit the spin operators in the local reference frame become $\tilde{S}_i^+ = \sqrt{2S} b_i$, $\tilde{S}_i^- = \sqrt{2S} b_i^\dagger$, and $\tilde{S}_i^z = S - b_i^\dagger b_i$, where b_i and b_i^\dagger are the boson (magnon) annihilation and creation operators, respectively. Retaining only the quadratic terms in b and b^\dagger , which describe the dynamics of the noninteracting magnons and neglect magnon interaction terms of order $1/S$, the generalized Hamiltonian [Eq. (4)] reduces to

$$\mathcal{H} = \sum_{\langle ij \rangle} [\mathcal{J}_{ij} (G_{ij}^1 b_i^\dagger b_j + G_{ij}^2 b_i b_j + \text{H.c.}) + f_{ij} (b_i^\dagger b_i + b_j^\dagger b_j)], \quad (5)$$

where $\mathcal{J}_{ij} = SJ_{ij}/2$, $f_{ij} = -SJ_{ij} F_{ij}^{zz}$, and the rotation coefficients $G^z = (F_{ij}^{xx} \pm F_{ij}^{yy}) - i(F_{ij}^{xy} \mp F_{ij}^{yx})$. The Hamiltonian (5) is diagonalized by the Bogoliubov transformation

$$b_i = \sum_n (u_n^i c_n + v_n^{i*} c_n^\dagger), \quad (6)$$

where c^\dagger and c are the quasiparticle operators. u and v , which satisfy $\sum_n (u_n^i u_n^{j*} - v_n^{i*} v_n^j) = \delta_{ij}$, ensuring the bosonic character of the quasiparticles are obtained from the Bogoliubov-de

Genes (BdG) equation

$$\begin{pmatrix} A_{ij} & B_{ij}^* \\ B_{ij} & A_{ij}^* \end{pmatrix} \begin{pmatrix} u_n^j \\ v_n^j \end{pmatrix} = \omega_n \begin{pmatrix} \delta_{ij} & 0 \\ 0 & -\delta_{ij} \end{pmatrix} \begin{pmatrix} u_n^j \\ v_n^j \end{pmatrix}, \quad (7)$$

where $A_{ij} = 2\mathcal{J}_{ij}(G_{ij}^1 + G_{ji}^{1*}) + \epsilon_i\delta_{ij}$, $B_{ij} = 2\mathcal{J}_{ij}(G_{ij}^2 + G_{ji}^{2*})$, and $\epsilon_i = 2\sum_j(f_{ij} + f_{ji})$. Now the spin-spin correlation function can be evaluated using the magnon energies and wave functions obtained from Eq. (7), where the excitation eigenvalues $\omega_n \geq 0$.

B. Dynamical structure factor

A neutron scattering experiment measures the spin-spin correlation function in Fourier and frequency space $D(\mathbf{k}, \omega)$ to describe the spin dynamics of the magnetic systems on an atomic scale. From $\mathbf{S}_i = U_i^{-1}\bar{\mathbf{S}}_i$ one can express $S_i^\alpha = \sum_\mu U_i^{\mu\alpha} \bar{S}_i^\mu$, where α and μ represent the x , y , and z components. Now applying the approximate HP transformation to the rotated spins, one can write

$$S_i^\beta = p_i^\beta b_i + q_i^\beta b_i^\dagger + r_i^\beta (S - b_i^\dagger b_i), \quad (8)$$

where $\beta = +, -, \text{ and } z$, and p, q , and r are the rotation coefficients (given in the Appendix).

Putting Eq. (6) in Eq. (8) the space-time spin-spin correlation function can be written as

$$S_i^\alpha(t)S_j^\beta(0) = \sum_{mn} \left[A_{mn}^{\alpha\beta} c_m^\dagger(t)c_n(0) + B_{mn}^{\alpha\beta} c_m(t)c_n^\dagger(0) \right], \quad (9)$$

where the coefficients A and B are expressed in the Appendix. In Fourier and frequency space,

$$D^{\alpha\beta}(\mathbf{k}, \omega) = \frac{1}{N} \int dt e^{i\omega t} \sum_{ij} e^{i\mathbf{k}\cdot(\mathbf{r}_i - \mathbf{r}_j)} \langle S_i^\alpha(t)S_j^\beta(0) \rangle. \quad (10)$$

The general expression for inelastic magnetic scattering is¹³

$$D(\mathbf{k}, \omega) = \sum_{\alpha\beta} \left(\delta_{\alpha\beta} - \frac{k_\alpha k_\beta}{k^2} \right) D^{\alpha\beta}(\mathbf{k}, \omega).$$

This general expression, arising from correlators of the form $\langle S_i^\alpha(t)S_j^\beta(0) \rangle$, where the (α, β) can be x, y, z , simplifies considerably in our case. (i) For a model as ours, Eq. (2), where S_z^{tot} is a constant of motion, mixed correlators of the form $\langle S_x S_y \rangle$, etc., vanish¹³. This would leave only the ‘‘diagonal’’ correlators, $\langle S_x(t)S_x(0) \rangle$, $\langle S_y(t)S_y(0) \rangle$, and $\langle S_z(t)S_z(0) \rangle$. (ii) Among these, the zz correlation does not contribute¹³ to inelastic scattering within linear SW theory.

As a result the relevant spin-spin correlation function, for us, becomes

$$\begin{aligned} D(\mathbf{k}, \omega) &= \frac{1}{2} [D^{+-}(\mathbf{k}, \omega) + D^{-+}(\mathbf{k}, \omega)] \\ &= \sum_l W_{\mathbf{k}}^l \delta(\omega - \omega_l), \end{aligned} \quad (11)$$

where the coefficient of the delta function

$$W_{\mathbf{k}}^l = \frac{1}{N} \sum_{ij} \mathcal{B}_{ij}^l e^{i\mathbf{k}\cdot(\mathbf{r}_i - \mathbf{r}_j)}$$

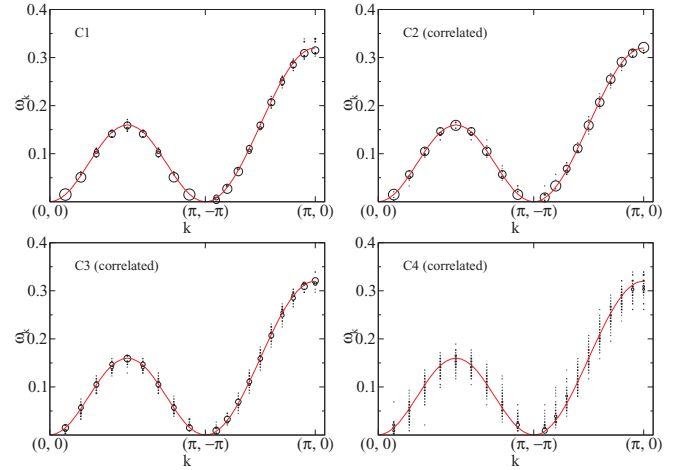


FIG. 3. (Color online) Spin-wave spectra along the main symmetry directions of the Brillouin zone for spin configurations C1, C2, C3, and C4 ($x = 0.01, 0.07, 0.21$, and 0.41 , respectively, shown in Fig. 1). With increasing ASD from C1 to C4 the spectrum becomes broader for a fixed value of momentum \mathbf{k} . Here $J_F = -0.04$, $J_{AF} = 0.065$, and the lattice size is 40×40 .

is the SW weight with $\mathcal{B}_{ij}^l = \frac{1}{2}(B_{ij}^{+-} + B_{ij}^{-+}) + B_{ij}^{zz}$. $W_{\mathbf{k}}^l$ is observed as the intensity of the magnon spectrum in the neutron scattering experiment.

IV. RESULTS AND DISCUSSION

We start by presenting the results for magnons in the configurations C1–C4 shown in Fig. 1 and then move to an analysis of the linewidth, the estimation of domain size, and the contrast with the uncorrelated disordered case.

A. Antiferromagnetically coupled domains

Figure 3 shows the magnon spectra of C1–C4 obtained from the Heisenberg model with the FM and AFM couplings discussed earlier, where the circles with different sizes are proportional to the intensities of the corresponding magnon modes. In a model with only FM couplings, i.e., no disorder, we would have obtained only the red curve, $\omega_{\mathbf{k}}^0$, for propagating magnons. The striking feature in all these panels is how closely the mean energy of the magnons follows $\omega_{\mathbf{k}}^0$ despite the large degree of mislocation in C2 and C3 and maximal disorder ($x \sim 0.4$) in C4 (refer to the spatial plots in Fig. 1). The broadening, although noticeable in C4, does not obscure the basic dispersion.

Figure 4 quantifies the mean energy and broadening by computing

$$\begin{aligned} \bar{\omega}_{\mathbf{k}} &= \int D(\mathbf{k}, \omega) \omega d\omega \quad \text{and} \\ [\Delta\omega_{\mathbf{k}}]^2 &= \left[\int D(\mathbf{k}, \omega) \omega^2 d\omega \right] - \bar{\omega}_{\mathbf{k}}^2, \end{aligned}$$

respectively. We have shown these two quantities for the C2–C4 structures in Fig. 4. The $\bar{\omega}_{\mathbf{k}}$ have been vertically shifted for clarity and the $\Delta\omega_{\mathbf{k}}$ are superposed as *error bars* on these. It is clear that even in the most disordered sample (C4), where the mislocation $x \sim 0.4$, the broadening is only a small fraction of

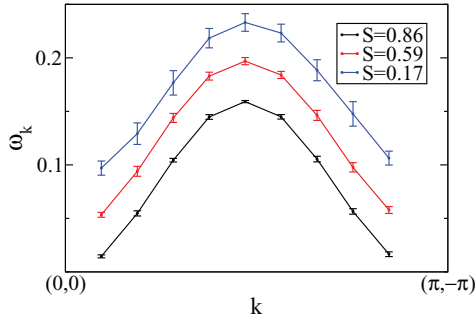


FIG. 4. (Color online) Mean spin-wave energy $\bar{\omega}_k$ (dots) and the spin-wave width $\Delta\omega_k$ (bars) for the correlated antisite configurations C2–C4 with *coupled domains*. The curves are vertically shifted for clarity.

the magnon energy. This will be an indicator when we discuss spin waves in an uncorrelated disordered background.

B. Broadening: Impact of domain size

There are two ingredients responsible for the spectra that one observes in Fig. 3: (i) The domain structure and (ii) the AFM coupling across the domains. To deconvolve these effects and have a strategy for inferring domain size from the neutron-scattering data, we studied a situation where we set $J_{AF} = 0$ in the Heisenberg model defined on the structures C1–C4. In that case we will have *decoupled ferromagnetic domains* without any antiparallel spin orientation between them. We think this is an interesting scheme to explore since the AFM bonds are limited to the domain boundaries and *is not* equal to the number of mislocated sites.

Figure 5 shows the overall magnon spectra for this case, using the same convention as in Fig. 3, while Fig. 6 quantifies the mean energy and broadening in this “decoupled domain” case. The absence of J_{AF} does not seem to make a significant

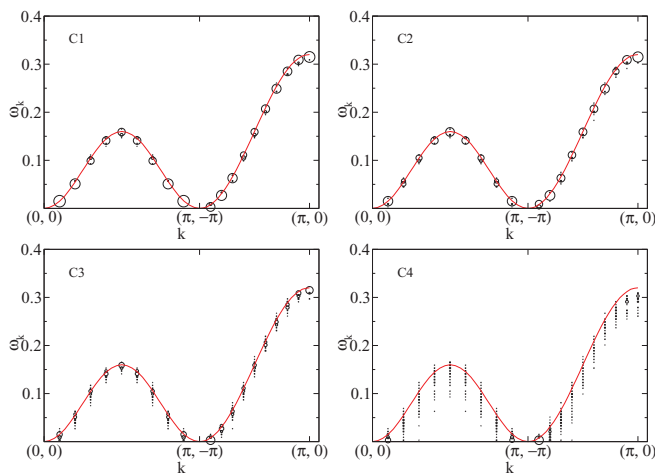


FIG. 5. (Color online) Spin-wave spectra along the main symmetry directions of the Brillouin zone for spin configurations C1–C4 (Fig. 1) with $x = 0.01, 0.07, 0.21,$ and 0.41 , respectively. Increasing the fractional weakly coupled domain boundary spins from C1 to C4 enhances the spin-wave softening near the zone boundary along $[\pi,0]$ and the spectrum also becomes broader for a given k . Here $J_F = -0.04$, $J_{AF} = 0$, and the lattice size is 40×40 .

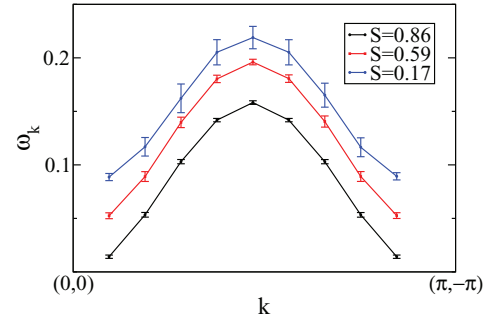


FIG. 6. (Color online) Mean spin-wave energy $\bar{\omega}_k$ (dots) and the spin-wave width $\Delta\omega_k$ (bars) for the correlated antisite configurations C2–C4 with *decoupled domains* ($J_{AF} = 0$). The curves are vertically shifted for clarity.

difference to the spectrum, as a comparison of Figs. 4 and 6 reveals. This correspondence, valid even in C4, suggests the following: (i) Most of the spectral features arise from the domain structure, and the associated confinement of spin waves, rather than the AFM coupling, and (ii) we can proceed with a much simpler modeling of the spectrum and estimation of domain size without invoking the complicated BdG formulation that AFM coupling requires.

Essentially, much can be learned from *tight binding* models defined on appropriate structures, as does happen for FM states, without having to invoke the “pairing” terms that arise for AFM coupling. A modeling of the full dispersion will require the AFM terms as well, but the inference about the presence of domains, and an estimate of their size, need not. We proceed with this next.

To estimate the typical domain size we need a few assumptions: (i) The total degree of mislocation x should be known, based on the bulk magnetization measurement. (ii) If the overall system size in $L \times L$ [or equivalent in a three-dimensional model], the number of mislocated sites

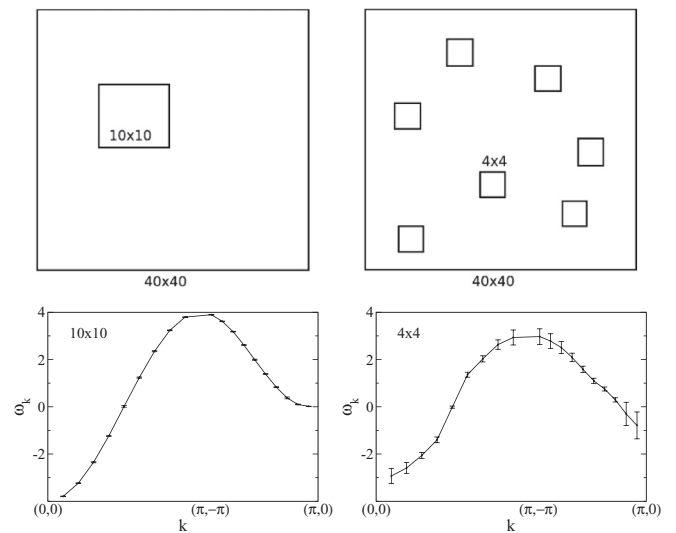


FIG. 7. Modeling of configuration C2 in terms of a domain of size 10×10 (left) and of seven domains of size 4×4 (right). The corresponding mean energy and broadening are shown below.

would be xL^2 . (iii) If the domain size is L_d , then the number of domains within the $L \times L$ area is $N_d \sim xL^2/L_d^2$. In reality domains need not have one single size, as C2–C4 indicate, but we need the assumption to make some headway. (iv) We need to locate these N_d domains randomly, in a nonoverlapping manner, within the $L \times L$ system, and average the spectrum obtained over different realizations of domain location.

This scheme, carried out for various L_d , can be compared to the full $D(\mathbf{k}, \omega)$ data to get a feel for the appropriate L_d . We show the result in Fig. 7 for such a tight binding exploration for the C2 configuration, modeled in terms of different domain distributions that respect the same overall mislocation.

When we compare the ratio of mean broadening to bandwidth obtained at different values of L_d (and so N_d) with that for the real data (Fig. 4), it turns out that $L_d = 10$ provides a best estimate. It also reasonably describes the broadening at stronger disorder, C3 and C4, where of course N_d is larger. An analytic feel for these results can be obtained by considering the modes of a square size $L_d \times L_d$ under open boundary conditions.

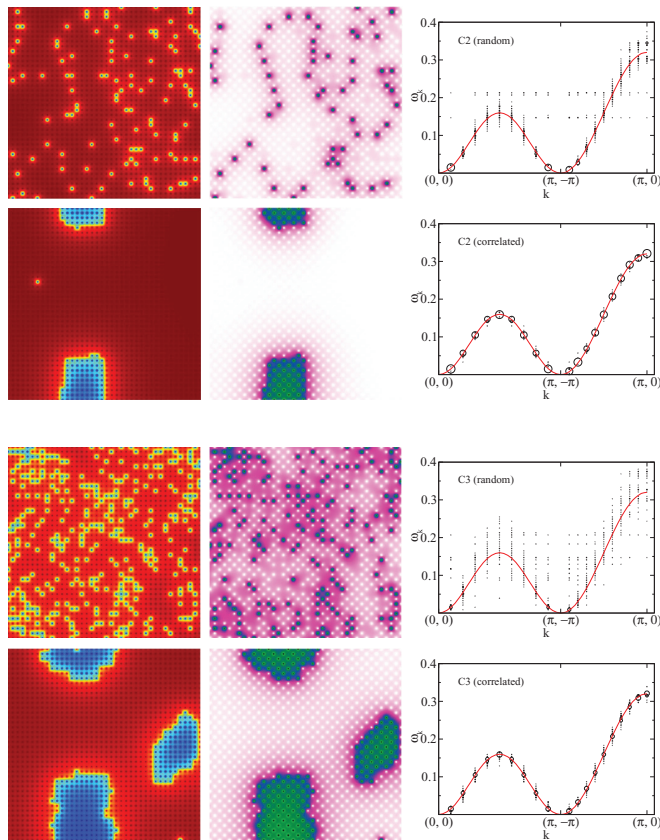


FIG. 8. (Color online) The top set of panels corresponds to mislocation $x = 0.07$ (C2) where we compare the magnon spectrum for an uncorrelated disordered case (above) with a correlated disordered case (below). The left panels refer to the structural pattern, the middle to the magnetic ground state, and the right to the magnon response. The bottom set of panels corresponds to $x = 0.21$ (C3), and the same indicators as for the top panels. Notice the remarkably broader lineshape for the uncorrelated disordered case where it is difficult to make much of a correspondence with the clean dispersion.

C. Contrast with uncorrelated antisites

In modeling the antisite disorder much of the earlier work in the field assumed the defect locations to be random. We have followed the experimentally motivated path which suggests that the mislocated sites themselves form an ordered structure separated from the parent (or majority) by an antiphase boundary. The sources of scattering are the boundaries between these domains rather than random point defects. Since much of double perovskite modeling has assumed the random antisite situation it is worth exploring the differences in the magnon spectrum between correlated and uncorrelated antisites.

We have already seen the results for correlated disorder for different degrees of mislocation x . We generated *uncorrelated* antisite configurations with the same x by starting with ordered configurations and randomly exchanging B and B' until the desired degree of disorder is reached. These configurations naturally do not have any structural domains. Annealing the full electronic Hamiltonian on these configurations, call them C1 (random), C2 (random), \dots , etc., down to low T , leads to the magnetic ground states. The ground states are disordered ferromagnets but without any domain pattern. We computed the magnon lineshape in these configurations, and, for illustration, show the results for C2 (random) and C3 (random) above and below, respectively, with their correlated counterparts C2 and C3 (Fig. 8).

There is a *striking increase* in the magnon linewidth (or $\Delta\omega_{\mathbf{k}}$) in the uncorrelated case. There is an almost ninefold increase in the magnon linewidth in C2 and sixfold in C3 of the uncorrelated disordered case with respect to the correlated disordered case.

V. CONCLUSIONS

We have studied the dynamical magnetic structure factor of a double perovskite system, taking into account the basic ferromagnetic ordering tendency and the defect induced local antiferromagnetic correlations. We used structural motifs that correspond to correlated disorder, obtained from an annealing process using a Monte Carlo method. The magnon excitations are calculated for an effective Heisenberg model within a $1/S$ expansion using the spin-rotation technique, with the ferromagnetic and antiferromagnetic couplings of the Heisenberg model obtained by a fit to T_c scales of the full electronic Hamiltonian. Our results on magnon energy and broadening reveal the following: (i) Even at very large disorder, the existence of a domainlike structure ensures that the response has a strong similarity to the clean case. (ii) Most of the spectral features arise from the domain confinement of magnon modes and we suggest a scheme for inferring the domain size from the spin-wave damping, so that experimenters can make an estimate of domain size without access to spatial information. (iii) The assumption about random antisites, which is widely used in modeling these materials, leads to a gross overestimate of magnon damping. In summary, dynamical neutron scattering can be a direct probe of the unusual ferromagnetic state in these materials and confirms the presence of antisite domains and yields information on their size. This would be vital in resolving the puzzle between “local order” and “global disorder” that seems pervasive in these materials.

ACKNOWLEDGMENTS

We acknowledge use of the High Performance Computing facility at HRI and discussions with G. V. Pai, S. Datta, and R. Tiwari. P.M. thanks the DAE-SRC Outstanding Research Investigator grant, and the DST India (Athena) for support.

APPENDIX

The rotation coefficients are

$$p_i^\pm = \sqrt{\frac{S}{2}}(U_i^{xx} \pm U_i^{yy}) - i(U_i^{yx} \mp U_i^{xy}),$$

$$q_i^\pm = \sqrt{\frac{S}{2}}(U_i^{xx} \mp U_i^{yy}) + i(U_i^{yx} \pm U_i^{xy}),$$

$$r_i^\pm = U_i^{zx} \pm iU_i^{zy},$$

$$p_i^z = U_i^{xz} - iU_i^{yz},$$

$$q_i^z = U_i^{xz} + iU_i^{yz}, \quad \text{and}$$

$$r_i^z = U_i^{zz}.$$

The structure factor coefficients are

$$A_{mn}^{\alpha\beta} = q_i^\alpha p_j^\beta u_i^{m*} u_j^n + p_i^\alpha q_j^\beta v_i^{m*} v_j^n + p_i^\alpha p_j^\beta v_i^{m*} u_j^n$$

$$+ q_i^\alpha q_j^\beta u_i^{m*} v_j^n - S \times r_i^\alpha r_j^\beta (u_i^{m*} u_i^n + u_j^{m*} u_j^n) \quad \text{and}$$

$$B_{mn}^{\alpha\beta} = q_i^\alpha p_j^\beta v_i^m v_j^{n*} + p_i^\alpha q_j^\beta u_i^m u_j^{n*} + p_i^\alpha p_j^\beta u_i^m v_j^{n*}$$

$$+ q_i^\alpha q_j^\beta v_i^m u_j^{n*} - S \times r_i^\alpha r_j^\beta (v_i^m v_i^{n*} + v_j^m v_j^{n*}).$$

*Present address: Department of Physics, Techno India University, Salt Lake Campus, Kolkata 700 091, India; skdiitk@gmail.com

¹For reviews, see D. D. Sarma, *Curr. Opin. Solid State Mater. Sci.* **5**, 261 (2001); D. Serrate, J. M. De Teresa, and M. R. Ibarra, *J. Phys.: Condens. Matter* **19**, 023201 (2007).

²K.-I. Kobayashi, T. Kimura, H. Sawada, K. Terakura, and Y. Tokura, *Nature (London)* **395**, 677 (1998).

³Y. Tomioka, T. Okuda, Y. Okimoto, R. Kumai, K.-I. Kobayashi, and Y. Tokura, *Phys. Rev. B* **61**, 422 (2000).

⁴T. Asaka, X. Z. Yu, Y. Tomioka, Y. Kaneko, T. Nagai, K. Kimoto, K. Ishizuka, Y. Tokura, and Y. Matsui, *Phys. Rev. B* **75**, 184440 (2007).

⁵C. Meneghini, S. Ray, F. Liscio, F. Bardelli, S. Mobilio, and D. D. Sarma, *Phys. Rev. Lett.* **103**, 046403 (2009).

⁶M. Hennenon, F. Moussa, P. Lehouelleur, F. Wang, A. Ivanov, Y. M. Mukovskii, and D. Shulyatev, *Phys. Rev. Lett.* **94**, 057006 (2005).

⁷S. Petit, M. Hennenon, F. Moussa, D. Lamago, A. Ivanov, Y. M. Mukovskii, and D. Shulyatev, *Phys. Rev. Lett.* **102**, 207201 (2009).

⁸P. Sanyal, S. Tarat, and P. Majumdar, *Eur. Phys. J. B* **65**, 39 (2008).

⁹V. N. Singh and P. Majumdar, *Europhys. Lett.* **94**, 47004 (2011).

¹⁰S. Kumar and P. Majumdar, *Eur. Phys. J. B* **50**, 571 (2006).

¹¹G. Jackeli, *Phys. Rev. B* **68**, 092401 (2003).

¹²J. T. Haraldsen and R. S. Fishman, *J. Phys.: Condens. Matter* **21**, 216001 (2009).

¹³S. W. Lovesey, *Theory of Neutron Scattering from Condensed Matter: Volume 2* (Clarendon Press, Oxford, UK, 1984).